ENSO impacts on global yields of major crops projected by a climate-crop model ensemble

John Harrington-Tsunogai [1, 2], Michiya Hayashi [3], Hideo Shiogama [3], Takahiro Takimoto [1], Wonsik Kim [1], Toshichika Iizumi [1, *]

[1] National Agriculture and Food Research Organization, 3-1-3 Kannondai, Tsukuba, Ibaraki 305-8604 Japan
[2] College of Geoscience, School of Life and Environmental Sciences, University of Tsukuba, 1-1-1 Tennodai, Tsukuba, Ibaraki 305-8577 Japan
[3] National Institute for Environmental Studies, 16-2 Onogawa, Tsukuba, Ibaraki 305-8506 Japan

Correspondence: Toshichika Iizumi (iizumit@affrc.go.jp)

Running page head:
Projected ENSO impacts on global yields

ABSTRACT

The El Niño–Southern Oscillation (ENSO) likely continues to be the main mode of natural climate variability in a warmer climate. However, it is currently not known how the ENSO impacts on major crop yields would change in response to future climate change. Here, we present the projected ENSO impacts on yields of maize, wheat, rice and soybean in the middle (2035–2064) and end (2065–2094) of the 21st century under low (SSP126) and high (SSP585) warming scenarios. The climate-crop model ensemble used is limited in its ability to simulate the historical ENSO impacts, with variation by crop and ENSO phase. Particularly, the model ensemble's ability was found to be low for rice and soybean. Consequently, the analysis presented here is restricted to wheat in the La Niña years and maize in the El Niño and La Niña years. The results indicate that ENSO would continue to be a noticeable driver of yield variations, both positively and negatively, for some crops and regions. For example, we detect projected positive maize yield impact in North America and the negative maize yield impact in eastern Brazil due to El Niño, although these projected impacts vary by time period and warming levels. Improvements to both climate and crop models are required to capture the process chains from ocean to atmosphere to agro-environment to crop productivity and help cropping systems better prepare for future climate risks.

KEY WORDS: Agriculture, Climate change, Climate impact, Climate variability, Global gridded crop model

1. INTRODUCTION

The El Niño–Southern Oscillation (ENSO) is a major mode of natural climate variability that generally occurs once every few years. ENSO affects many natural and managed systems globally, including crop production by modulating growing season weather patterns, and can trigger multi-breadbasket crop failures (Iizumi et al. 2014, Anderson et al.2019, Heino et al. 2020, Anderson et al. 2023). The ENSO impacts on crop yields have implications for international food trade and the acute food insecurity in vulnerable regions of the world and are therefore of interest to governmental and commercial entities (FAO 2016, Ubilava 2017, GEOGLAM 2023, Koo & Anderson, 2023).

While there is literature on the ENSO impacts in the historical past, to the best of our knowledge, it remains unclear how the yield impacts associated with ENSO would change in response to projected warming. Projected changes in ENSO behavior have been intensively studied using ensemble simulations of global climate models (GCMs). The accumulated evidence suggests that the ENSO will remain the main mode of interannual climate variability in a warmer world (Arias et al. 2021, Singh et al. 2022, Vaittinada Ayar et al. 2023) and most climate models tend to show an ENSO amplification in the end of the 21st century (Cai et al. 2022).

To fill the knowledge gap, this study presents the global analysis of the ENSO impacts on yields of major crops in the middle (2035–2064) and end (2065–2094) of the 21st century under two emission scenarios from the Shared Socioeconomic Pathways (SSPs)–Representative Concentration Pathways (RCPs): SSP1–RCP2.6 (SSP126) and SSP5–RCP8.5 (SSP585). The former and latter represent low and high warming scenarios, respectively. We employed the recent climate-crop model ensemble, consisting of 12 global gridded crop models (GGCMs), provided by the Agricultural Model Intercomparison and Improvement Project (AgMIP)'s Global Gridded Crop Model Intercomparison (GGCMI) and the Intersectoral Impact Model Intercomparison (ISIMIP) project phase 3 (Jägermeyr et al. 2021). We studied four major crops—maize, wheat, rice and soybean—that produce nearly two-thirds of global agricultural calories (Tilman et al. 2011).

The main questions addressed in this study are: (i) How well does the historical simulation of the climate–crop model ensemble represent the actual ENSO impacts, particularly average yield changes in El Niño (La Niña) years relative to neutral years? and (ii) What are the potential differences in ENSO impacts under the two warming levels and across the two future time periods?

2. METHODS

2.1. Climate-crop model ensemble

2.1.1. Data

We used the GGCMI multi-GGCM ensemble mean percent yield change projections (Jägermeyr et al. 2021, Jägermeyr et al. 2024). The data provided annual changes in yields of the four crops for the period 1983–2099, relative to the 1983–2013 baseline, at 0.5° resolution. To derive the yield projections, the bias-corrected daily outputs of five GCMs (Table S1 in ELECTRONIC SUPPLEMENTS) under high and low emission scenarios were used to force the GGCMs. The emission scenarios were the SSP126 and SSP585. The former represents a scenario with low greenhouse gas emissions and sustainable development, while the latter corresponds to a high-emission pathway characterized by rapid economic growth and intensive greenhouse gas emissions. The average percent yield change data of the 12 GGCMs were available for the current global harvested area for each crop; though, not all GGCMs provided projections for every crop (Table 1).

Among the five available GCMs, we selected the yield projections forced by two GCMs, MPI-ESM1-2-HR and MRI-ESM2-0, for use. We were aware of the "hot model" problem that several Coupled Model Intercomparison Project Phase 6 (CMIP6) GCMs which have very high equilibrium climate sensitivity (ECS) overestimate future warming (Hausfather et al. 2022). ECS is the change in global surface temperature relative to preindustrial levels when the atmospheric CO_2 concentration doubles from 280 to 560 ppm and the Earth's climate reaches a new equilibrium state. The five GCMs used in the GGCMI multi-GGCM ensemble were a subset of CMIP6 GCMs designed to sample their ECS range (1.83°C to 5.67°C; IPCC 2021) as broadly as possible for impact studies (Lange 2021). The two GCMs selected for this study were at the lower end in terms of ECS (MPI-ESM1-2-HR, 2.98 °C; MRI-ESM2-0, 3.15 °C; Table S1), which is interpreted as a low risk of overestimating future warming for the GCMs.

Table 1. List of the GGCMs and modeling groups participating to the multi-GGCM ensemble average yield change dataset used for this study (Jägermeyr et al 2021).

GGCM name	Main modeling group	Note	Ref.
ACEA	University of Twente, The Netherlands	-	Mialyk et al. (2022)
CROVER	National Institute for Environmental Studies, Japan	-	Okada et al. (2018)
CYGMA (1p74)	National Agriculture and Food Research Organization, Japan	no wheat	Iizumi et al. (2017)
DSSAT-Pythia	University of Florida, USA	no rice	Hoogenboom et al. (2019)
EPIC-IIASA	International Institute for Applied Systems Analysis, Austria	-	Balkovič et al. (2014)
ISAM	University of Illinois, USA	-	Lin et al. (2021)
LandscapeDNDC	Karlsruhe Institute of Technology, Germany	-	Haas et al. (2012)
LPJmL	Potsdam Institute for Climate Impact Research, Germany	-	Von et al. (2018)
pDSSAT	Columbia University, University of Chicago, USA	-	Elliott et al. (2014)
PEPIC	Swiss Federal Institute of Aquatic Science and Technology, Switzerland	-	Liu et al. (2016)
PROMET	Ludwig-Maximilians-Universität München, Germany	-	Mauser et al. (2015)
SIMPLACE-LINTUL5+	Leibniz Centre for Agricultural Landscape Research, Germany	no rice	Webber et al. (2018)

2.1.2. Spatial imputation

To adjust the yield projections to a 2010 baseline, we used SPAM2010 (Yu et al. 2020), which provides yields for the year 2010 (the average of 2009–2011). However, it was found that there were missing values in the percent yield change data in some parts of the global harvested area in 2010. This was probably due to the inconsistencies between the global harvested area map used in the calculation of the multi-GGCM ensemble and SPAM2010 used in this study. We therefore spatially interpolated the data to fill the gaps.

To do this, we built random forest (RF) models that estimate the percent yield change from the geographic information (longitude, latitude and elevation). The specific RF model was developed for each combination of crop, year, warming level and GCM and then estimated missing values for a given combination. The statistical software R (R Core Team 2024) was used for the model fitting. We used the *randomForest* package (Liaw & Wiener 2022) and the package's default hyperparameter values, namely, number of trees (ntree)=500, number of predictors sampled at each split (mtry)=3 and minimum size of terminal nodes (nodesize)=5. When out-of-bug samples were evaluated, the model fit was as high as 0.60 (rice), 0.65 (wheat), 0.70 (maize) and 0.80 (soybean) for the coefficient of determination, and as low as 6.9 (rice), 7.7 (soybean), 8.0 (maize) and 9.5 (wheat) in units of percent point for the root-mean-squared residuals.

2.1.3. Baseline harmonization

After the spatial imputation, the yield projections were harmonized to have the 2010 baseline instead of the original 1983–2013 baseline. We harmonized the yield projections to match the SPAM2010 dataset. This alignment ensures consistency with SPAM2010.

Here we have two baseline periods. The first one was 1983–2013 and the second one was 2009–2011. The percent yield change for the year t relative to the first baseline period ($\%YC_1$) was given by:

$$\%YC_{1,t} = \frac{Y_t - \overline{Y_1}}{\overline{Y_1}} \times 100, \quad (1)$$

where Y is the annual yield (t ha^{-1}); $\overline{Y}$ is the average yield for the given baseline period (t ha^{-1}). Similar to above, the percent yield changes relative to the second baseline period ($\%YC_2$) was written as:

$$\%YC_{2,t} = \frac{Y_t - \overline{Y_2}}{\overline{Y_2}} \times 100. \quad (2)$$

Here yield anomaly in units of tones per hectare was respectively given by:

$$\Delta Y_{1\,t} = Y_t - \overline{Y_1} \text{ and } \Delta Y_{2\,t} = Y_t - \overline{Y_2}. \quad (3)$$

With the assumption that $\Delta Y_{1\,t} = \Delta Y_{2\,t}$, it was possible to convert the percent yield change value from the first baseline period to the second one:

$$\%YC_{2,t} = \left[\frac{\left(\frac{\%YC_{1,t} \cdot \overline{Y_1}}{100}\right)}{\overline{Y_2}}\right] \times 100 = \%YC_{1,t} \cdot \frac{\overline{Y_1}}{\overline{Y_2}}. \quad (4)$$

Although rare, the percent yield change value was replaced with –100% if the value calculated in the harmonization was negatively greater than this value. We thought that another assumption that $\%YC_{1,t}=\%YC_{2,t}$ was inappropriate for this study. As the average yield in the second baseline period (2010) was generally higher than that in the first baseline period (1983–2013), the absolute value of yield anomaly in tons per hectare calculated using the equal-percent-yield-change assumption became greater in the second baseline period than that in the first baseline period. Therefore, we selected to keep yield anomaly in tons per hectare the same between the first and second baseline periods.

The average yields of 1983–2013 ($\overline{Y_1}$) and 2009–2011 ($\overline{Y_2}$) were calculated using the country annual data available in the FAO statistical database (FAO 2024). Therefore, the harmonization we done was at the country level. At present, there is no global grid yield dataset that can be used for grid-wise harmonization. The global dataset of historical yields (GDHY) (Iizumi et al. 2014, Iizumi & Sakai 2000) has missing values for a non-negligible portion of the global cropland area. SPAM2000 has a base year of 2000 (You et al. 2014), which is not the same as the midpoint of the 1983–2013 period (i.e., 1998). More importantly, Yu et al. (2020) reports the presence of unrealistic disconnections in temporal change between SPAM2000 and SPAM2010 for some crops and regions, rooted in the different sources of information in the development of these datasets, which may ruin the harmonization.

2.1.4. Detrending

As elaborated in Jägermeyr et al. (2021), the percent yield change projections had long-term trends due to the changes in climate and atmospheric CO_2 concentration. Because the focus of the present study was on the yield impacts from ENSO, we distinguished between the interannual variability component of yield change, which was mainly driven by major climate mode (e.g., ENSO), and the trend component of yield change, which was associated with climate change. We calculated the 5-year running average series as the trend component and subtract it from the original percent yield change series to derive the interannual variability component (Fig. S1). Therefore, the percent yield anomalies studied here was the year-to-year deviation (affected by internal climate variability) from the long-term yield trends (affected by climate change).

2.2. Yield impacts by ENSO phase

2.2.1. ENSO index for CMIP6 GCMs

Using the CMIP6 multi-GCM ensemble climate dataset (Eyring et al. 2016), we calculated monthly mean sea surface temperature (SST) over the Nino3.4 region (5°S to 5°N and 170°W to 120°W) and their anomalies, relative the average of 1900–1999. As expected, the Nino3.4 monthly SST anomaly series showed an increasing trend in response to the projected warming. We therefore detrended them by using the locally weighted scatterplot smoothing (LOWESS) that is available in R (Cleveland et al. 1979) and distinguished the natural variability of monthly SST anomalies from the long-term trend (Fig. S2). The detrended Nino3.4 monthly SST anomaly series was calculated for each combination of the GCMs and warming levels and used as the ENSO index. This detrending procedure basically follows the method of Cai et al. (2022). However, we used LOWESS instead of the quadratic regression that is used in Cai et al. (2022) to allow detrending in a more non-parametric way.

2.2.2. Linking ENSO in the climate-crop model ensemble

We associated annual yield anomaly from long-term yield trend with ENSO phase following the method of Iizumi et al. (2014). The ENSO phases consist of three states: warm (El Niño), neutral and cool (La Niña). In addition, we made a distinction between strong and weak events for the warm phase based on the average of the detrended Nino3.4 monthly SST anomaly over three months before the harvest of a crop (ΔSST): a relatively strong El Niño ($\Delta SST > +1.0$ °C) and a relatively weak El Niño ($+0.5 < \Delta SST \leq +1.0$ °C). Similar to the warm phase, a distinction was made between a relatively strong La Niña ($\Delta SST < -1.0$ °C) and a relatively weak La Niña ($-1.0 < \Delta SST \leq -0.5$ °C). The remaining state was classified into a neutral phase ($-0.5 < \Delta SST < +0.5$ °C). Since weak El Niño and

La Niña events were few in the climate-crop model ensemble, as reported in Singh et al. 2022, the present study focused strong El Niño and La Niña events.

The harvest months for the crops considered here were obtained from the latest global crop calendars (Jägermeyr et al. 2021). Although the projected warming would accelerate crop growth, we used the fixed calendars throughout the study period as the multi-GGCM ensemble mean harvest months were not currently available. However, the observed advances in harvesting for the recent two decades are <2 weeks and the estimated change is <5 days per 1 °C warming (Hosokawa et al. 2023). As we associated the ENSO phase determined based on a 3-month average SST anomaly with yield anomaly, the assumption of time-constant crop calendars may not largely affect the results of this study.

2.2.3. Significance of the ENSO impacts

We respectively examined the statistical significance of yield impacts from the strong El Niño and strong La Niña years under the projected warming. To that end, the percent yield changes in the strong El Niño (La Niña) years were compared with those in the neutral years, with both samples consisting of the GCMs and years. We selected to combine the two GCMs (MPI-ESM1-2-HR and MRI-ESM2-0) to increase the sample size. The null hypothesis tested here using Welch's t-test (Welch 1947) was that the means of two populations are equal (i.e., the percent yield anomalies in the strong El Niño (La Niña) years and those in the neutral years have the same mean). This test can be applied to the case of different variance between two populations.

The significance testing was done for each crop, location and period. The historical period (1982–2020; 39 years) was relatively longer than the future period (2035–2064 and 2065–2094, each 30 years). This was because to compare with the historical ENSO impacts over as long a period as possible, and to have two non-overlapping time windows in the future period. The average sample size across the crops and warming levels, consisting of the GCMs and years, was {strong El Niño, Neutral, strong La Niña}={7.9, 50.2, 7.9} years in the historical period and {7.3, 45.6, 7.1} and {6.2, 49.1, 4.7} years for the middle and end of this century, respectively.

2.3. Climate-crop model ensemble performance

2.3.1. Actual ENSO-induced yield impacts

For validation purposes, we compared the ENSO impacts estimated using the climate-crop model ensemble in the historical period with the actual ones. The actual ENSO impacts were derived based on the GDHY grid yield dataset (Iizumi 2019, Iizumi & Sakai 2000), the reported crop calendars (Sacks et al. 2010) and the COBE2 (Centennial in Situ Observation-Based Estimates of the Variability of SST and Marine Meteorological Variables version 2) monthly SST dataset (Hirahara et al. 2014).

For consistent comparisons, annual yield data for the period 1981–2020 were detrended using the 5-year running averaging method. Then percent yield anomalies were calculated, relative to the average yields of 2009–2011, to have the 2010 baseline. In the GDHY dataset, yield data were available for two seasons for maize, rice and wheat (major and secondary seasons for maize and rice and winter and spring seasons for wheat), while only major season was available for soybean. We calculated average Nino3.4 SST anomaly over the three months before the harvest for each season of a crop when multiple seasons were operated. The calculated SST anomalies were further averaged across the seasons, when necessary. Annual yield anomalies were associated with the ENSO phase using the ENSO index calculated from the COBE2 SST dataset in the same manner as described for the climate-crop model ensemble.

2.3.2. Similarity in geographic patterns

To assess the reliability of the climate-crop model ensemble, we compared the spatial distributions of yield anomalies derived from the climate-crop model ensemble—based on the SSP126 scenario for the historical period with those actual data during El Niño and La Niña events. We used p-values, spatial correlations, and Cohen's kappa coefficients as metrics for this evaluation. As outlined in Section 2.2.3, p-values from Welch's t-test were used to gauge the significance of yield deviations during ENSO events relative to neutral years, with lower p-values indicating a more pronounced signal of ENSO impact. Spatial correlations were computed to assess the spatial agreement between the climate-crop model ensemble and actual data, while Cohen's kappa coefficients measured agreement in terms of the geographic patterns of categorical ENSO impacts (the significant positive/negative yield anomalies in each significance level).

3. RESULTS

3.1. Model ensemble performance

The performance reported here refers to how well the climate–crop model ensemble reproduces the actual (observed) yield anomalies under El Niño or La Niña conditions. Figure 1 illustrates how we assess the performance at different p-value thresholds, which were used to identify grid cells with a statistically significant difference (El Niño or La Niña vs. neutral). Specifically, for each threshold, we assess the spatial agreement with the observed yield anomalies in terms of spatial correlation and Cohen's kappa.

For illustrative purposes, we focus on El Niño impacts in the text below, but note the figure also covers La Niña impacts. As shown in the top left panel of Fig. 1, the number of grid cells identified with significant El Niño impacts decreases as the p-value threshold becomes more stringent (smaller). The skill score values (the spatial correlation and the kappa coefficient) gradually increase as the p-value becomes smaller, then drop for some crops if too few grid cells remain. This pattern suggests that the ensemble's performance is higher in regions with stronger, more consistent El Niño impacts. Maize shows this trend more clearly than other crops.

When the p-value was set as 0.1, consistent with the previous literature (Iizumi et al. 2014, Heino et al. 2020), the spatial correlation coefficients between the simulated and observed yield impacts for El Niño events were 0.63 for maize, –0.00 for rice, and –0.03 for wheat, while for La Niña events they were 0.29 for maize, 0.28 for rice, and 0.71 for wheat (see Table S2). The corresponding kappa values were 0.50, 0.01, and 0.17 for maize, rice, and wheat, respectively, during El Niño events, and 0.46, 0.25, and 0.59 during La Niña events. Notably, soybean showed negative correlations and kappa values for both ENSO phases, suggesting that the simulated yield deviations for soybean do not align well with the actual patterns. Overall, the model's performance also varies by ENSO phase: for example, the ensemble better captures La Niña impacts on wheat than El Niño impacts, whereas for maize and rice the differences between phases are less pronounced, with maize generally performing better than rice.

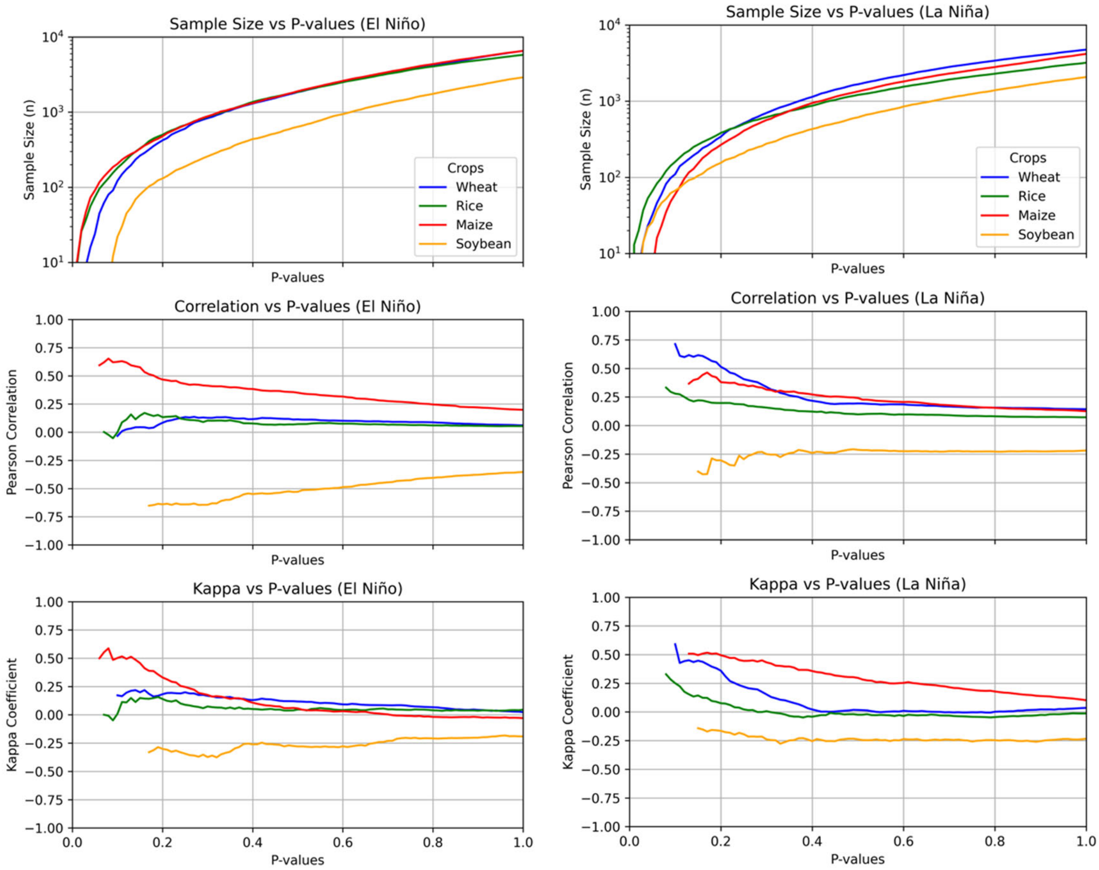

Fig. 1. Changes in the performance of climate-crop model ensemble with different p-value thresholds. The upper panels illustrate the number of grid cells with significant yield impact for a given significance level (i.e., p-value) for El Niño (left) and La Niña (right) phases during the historical period (1982–2020). The middle panels depict the relationship between the Pearson's spatial correlation coefficient and p-value thresholds for grid-cell yield impact. The bottom panels show the relationship between the kappa coefficient and p-value thresholds for grid-cell yield impact. These skill score values are shown only when 100 or more grid cells with significant yield impact are available.

3.2. Projected ENSO impacts on global yields

Concerning the reproductive performance of the climate-crop model ensemble described above, we limit our analysis of projected yield impact due to ENSO to the La Niña impacts on wheat and El Niño and La Niña impacts on maize (the results for wheat in the El Niño years and the El Niño and La Niña impacts for rice and soybean are available in Figs. S3–S7 for interested readers). Although the robust detection of projected ENSO impacts on yields is still challenging, some noticeable geographic patterns were found.

In the historical period, North America experienced a significant decrease in wheat yield in the La Niña years (Fig. 2). However, the negative impacts of La Niña in that region would be mitigated in the future regardless of the warming levels. Eastern Australia would experience the positive yield impacts from La Niña in the future, as did so in the historical period. In the other regions of the world, the projected La Niña impacts on wheat yield varied by the time periods and warming levels, making it difficult to depict concrete future trends.

For maize, North America showed a positive yield deviation when El Niño occurred in the climate-crop model ensemble, which was not well supported by the actual data (Fig. 3). The positive maize yield impact of El Niño in the region was projected to be weakened in the future. In Eastern Brazil, the negative maize yield deviation in the historical period would continue in the future, although it was projected to be mitigated in the end of this century under the high warming scenario. The projected results showed that the negative maize yield impacts of El Niño in South Africa may reverse in the future.

Historical data indicate that maize yield deviations during the La Niña phase are approximately opposite to those observed during the El Niño phase (Fig. 4). In North America, the negative yield deviation is projected to weaken by the end of this century. Additionally, eastern Brazil is expected to exhibit a larger area of positive yield deviation in the future.

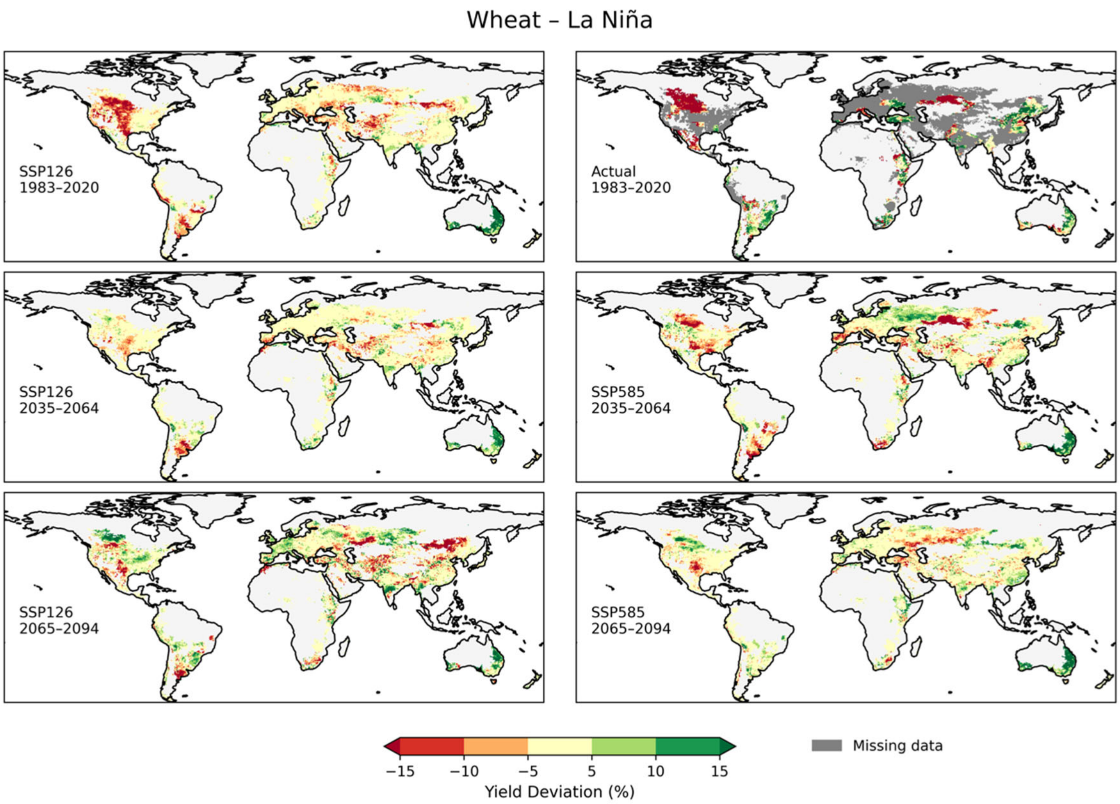

Fig. 2. The average percentage yield anomaly of wheat in La Niña years, relative to neutral years, for the historical (1983–2020) and future (2035–2064 and 2065–20940 periods. Two emission scenarios (SSP126 and SSP585) are considered for the future periods. The actual data are also shown for historical period. The red (green) shading indicates an increase (decrease) in average yield in La Niña years. For the historical period, only the result for the SSP126 scenario is shown to avoid redundancy.

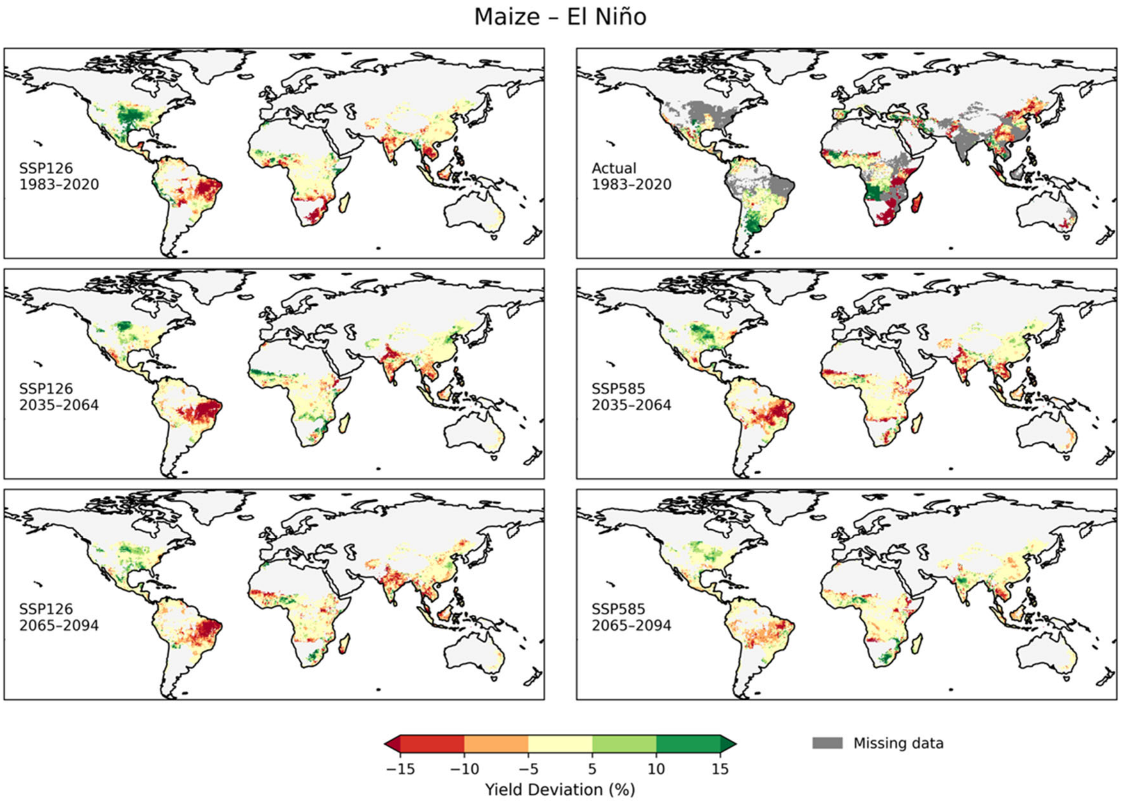

Fig. 3. Same as Fig. 2 but for maize in the El Niño years.

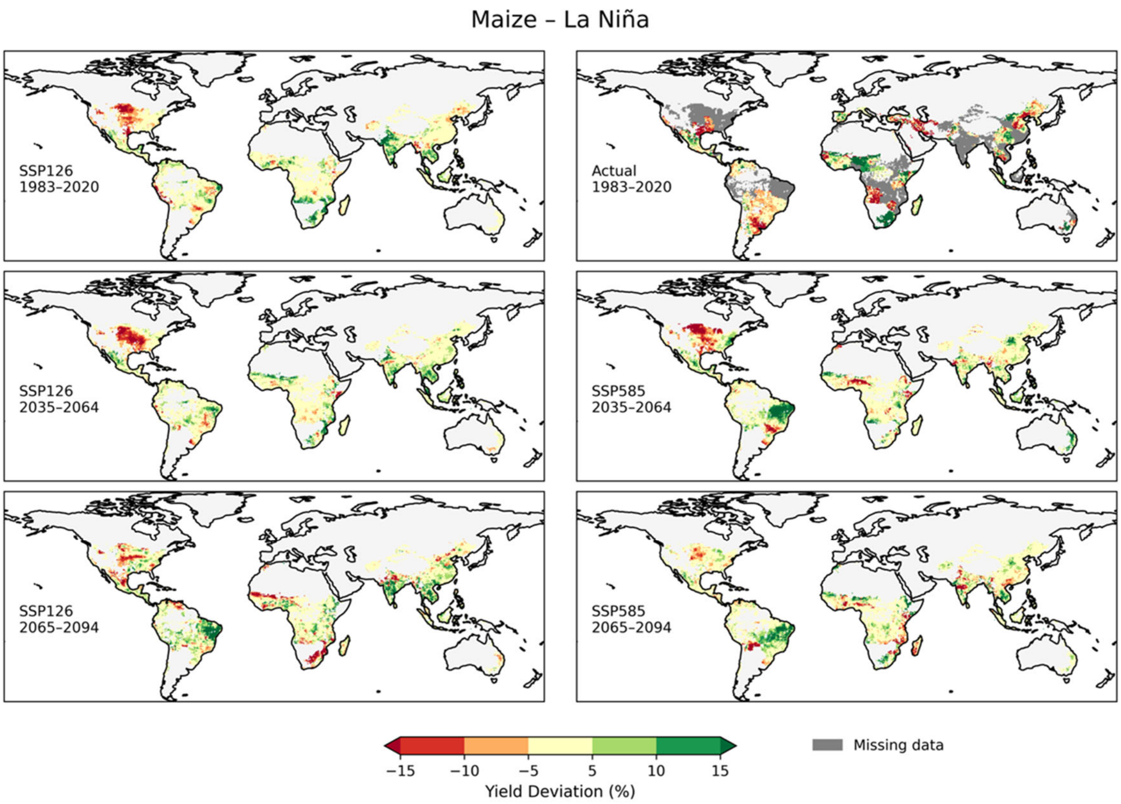

Fig. 4. Same as Fig. 2 but for maize in the La Niña years.

4. DISCUSSION

This study reveals that the current skill of the climate-crop model ensemble in reproducing the historical impacts of ENSO on global yields is limited. The ensemble performance varied considerably across crops and between ENSO phases. Interestingly, the historical ENSO impacts on average yield anomalies presented in this study shows a good agreement with that reported in Heino et al. (2019). However, discrepancies are seen in more regions when comparing the GGCM results reported in Heino et al. (2019) with the actual data. For instance, both agree on a strong decrease in yield in North America in the La Niña years, but in the El Niño years, the GGCM results reported in Heino et al. (2019) simulated an increase in yield, which is not supported by the actual data. However, note that the actual data derived based on GDHY dataset is suffer from missing information in many parts of the world (Table S3). This finding highlights the need for further improvement in both the climate-crop model ensemble and the grid yield dataset.

The results indicate that yield impacts associated with ENSO may not be fully represented by GGCMs. Our finding is in line with the result of Schewe et al. (2019) that the simulated damages due to extreme climate events are underestimated by current generation of GGCMs. This underestimation partly arises from an inadequate representation of processes in GGCMs, for instance, the availability of water for irrigation is limited when droughts occur (Schewe et al. 2019). This limitation of current GGCMs needs to be overcome to provide more reliable future projections on climate risks in food production.

In addition, GCMs have their own challenges. Recent studies have underscored profound uncertainties in ENSO predictions themselves. Hayashi et al, (2020) found that many GCMs underestimate subsurface nonlinear dynamical heating, a deficiency that leads to an underestimation of ENSO asymmetry and biases in simulating SST anomalies in the eastern equatorial Pacific. Similarly, Bayr & Latif (2022) demonstrated that the underestimation of key atmospheric feedback can induce compensating errors that distort the simulation of ENSO dynamics, including its asymmetry and phase locking to the seasonal cycle. Cai et al, (2021) reported that changes in the mean state of the equatorial Pacific, which are critical for modulating ENSO responses under greenhouse warming, are inconsistently represented across GCMs. Together, these deficiencies contribute to a large inter-GCM spread in projected ENSO behavior, ultimately affecting the reliability of ENSO impacts on yields in climate-crop model ensemble.

Despite the limitations, the climate-crop model ensemble provides some insights into the ENSO impacts on crop yields in the future. At least, it is likely that ENSO causes yield variations, both positively and negatively, for some crops and regions. However, disentangling the ENSO impact on global yields across different future time periods and warming levels proved challenging (Table S4). Future research should aim to clearly delineate how ENSO-induced oceanic variations trigger atmospheric changes, which in turn alter agro-environmental conditions and affect plant growth. This improved understanding of the entire process chain will enable more accurate projections of ENSO impacts on crop yields.

This study has several limitations. First, geographic distributions of harvested areas may shift in the future due to changing cultivation zones influenced by climate change and land-use dynamics driven by food demand and environmental policies, potentially altering the geographic patterns of ENSO impacts on yields. Second, uncertainties inherent in future climate projections and the current limitations of climate-crop models in capturing ENSO-induced yield variability highlight the need for further model improvement. Furthermore, the use of improved crop cultivars—more tolerant to suboptimal conditions such as heat, drought, and excessive soil moisture—could modify yield responses to ENSO, yet a fixed technological level was assumed in the current ensemble.

5. CONCLUSIONS

This study investigated the impacts of ENSO on global yields of major crops under projected future climate conditions using the recent climate-crop model ensemble. The reproductive performance of the model ensemble for the historical ENSO impacts considerably varied by crop and ENSO phase, with relatively good performance in wheat in La Niña years and maize in El Niño and La Niña years. Currently, the model performance is found to be poor for rice and soybean. These findings suggest that detecting the ENSO impacts on crop yields is challenging due to the complexities associated with the asymmetric performance between El Niño and La Niña events and the resulting teleconnections, as well as the different geographic distributions of harvested area, and different growing season between the crops. However, it is likely that the ENSO continues to be a noticeable driver of interannual yield deviation even in a warmer world. A better understanding of the complex interactions between ocean, atmosphere and crops is needed to improve our capacity to project future climate risks to food production, and ultimately to help societies better prepare for them.

Acknowledgements

This study was supported by the Environment Research and Technology Development Fund of the Environmental Restoration and Conservation Agency provided by the Ministry of the Environment of Japan (Grant Number: JPMEERF23S21120); and Grants-in-Aid for Scientific Research were received from the Japan Society for the Promotion of Science (22H00577 and 23H00351).

LITERATURE CITED

[1]. Anderson W, Baethgen W, Capitanio F et al. (2023) Climate variability and simultaneous breadbasket yield shocks as observed in long-term yield records. Agricultural and Forest Meteorology 331:109321. https://doi.org/10.1016/j.agrformet.2023.109321

[2]. Anderson WB, Seager R, Baethgen W et al. (2019) Synchronous crop failures and climate-forced production variability. Science Advances 5:eaaw1976. https://doi.org/10.1126/sciadv.aaw1976

[3]. Arias PA, Bellouin N, Coppola E et al. (2021) Technical summary. In: Masson-Delmotte V, Zhai P, Pirani A et al. (eds) Climate change 2021: the physical science basis. Contribution of Working Group I to the Sixth Assessment Report of the Intergovernmental Panel on Climate Change. Cambridge University Press, Cambridge (in press)

[4]. Balkovič J, van der Velde M, Skalský R et al. (2014) Global wheat production potentials and

management flexibility under the representative concentration pathways. Global and Planetary Change 122:107–121. https://doi.org/10.1016/j.gloplacha.2014.08.010

[5]. Cai W, Ng B, Wang G et al. (2022) Increased ENSO sea surface temperature variability under four IPCC emission scenarios. Nature Climate Change 12:228–231. https://doi.org/10.1038/s41558-022-01282-z

[6]. Cleveland WS (1979) Robust locally weighted regression and smoothing scatterplots. Journal of the American Statistical Association 74:829–836

[7]. Elliott J, Kelly D, Chryssanthacopoulos J et al. (2014) The parallel system for integrating impact models and sectors (PSIMS). Environmental Modelling & Software 62:509–516. https://doi.org/10.1016/j.envsoft.2014.04.008

[8]. Eyring V, Bony S, Meehl GA et al. (2016) Overview of the Coupled Model Intercomparison Project Phase 6 (CMIP6) experimental design and organization. Geoscientific Model Development 9:1937–1958. https://doi.org/10.5194/gmd-9-1937-2016

[9]. FAO (2016) 2015–2016 El Niño early action and response for agriculture, food security and nutrition. https://openknowledge.fao.org/server/api/core/bitstreams/643a2950-075d-46d6-ae39-d0d5abcc2c86/content (accessed 18 February 2025)

[10]. FAO (n.d.) FAOSTAT. https://www.fao.org/faostat/en/#data (accessed 11 Dec 2024)

[11]. GEOGLAM (2023) Crop Monitor for AMIS – June 2023. https://static1.squarespace.com/static/636c12f7f9c2561de642a866/t/65678074cccf4a69e9c8e0b5/1701281911595/AMIS_CropMonitor_202306.pdf (accessed 18 February 2025)

[12]. Haas E, Klatt S, Fröhlich A et al. (2013) LandscapeDNDC: a process model for simulation of biosphere–atmosphere–hydrosphere exchange processes at site and regional scale. Landscape Ecology 28:615–636. https://doi.org/10.1007/s10980-012-9772-x

[13]. Hausfather Z, Marvel K, Schmidt GA et al. (2022) Climate simulations: recognize the 'hot model' problem. Nature 605:26–29. https://doi.org/10.1038/d41586-022-01192-2

[14]. Heino M, Guillaume JHA, Müller C, Iizumi T, Kummu M (2020) A multi-model analysis of teleconnected crop yield variability in a range of cropping systems. Earth System Dynamics 11:113–128. https://doi.org/10.5194/esd-11-113-2020

[15]. Hirahara S, Ishii M, Fukuda Y (2013) Centennial-scale sea surface temperature analysis and its uncertainty. Journal of Climate 27:57–75. https://doi.org/10.1175/jcli-d-12-00837.1

[16]. Hoogenboom G, Porter CH, Boote KJ et al. (2019) The DSSAT crop modeling ecosystem. In: Boote KJ (ed) Advances in crop modeling for a sustainable agriculture. Burleigh Dodds Science Publishing, Cambridge, p 173–216. https://doi.org/10.19103/AS.2019.0061.10

[17]. Hosokawa N, Doi Y, Kim W et al. (2023) Contrasting area and yield responses to extreme climate contributes to climate-resilient rice production in Asia. Scientific Reports 13:6219. https://doi.org/10.1038/s41598-023-33413-7

[18]. Iizumi T (2019) GDHY_v1_2_v1_3 [Data set]. Data Integration and Analysis System (DIAS). https://doi.org/10.20783/DIAS.564

[19]. Iizumi T, Furuya J, Shen Z et al. (2017) Responses of crop yield growth to global temperature and socioeconomic changes. Scientific Reports 7:7800. https://doi.org/10.1038/s41598-017-08214-4

[20]. Iizumi T, Luo JJ, Challinor A et al. (2014) Impacts of El Niño Southern Oscillation on the global yields of major crops. Nature Communications 5:3712. https://doi.org/10.1038/ncomms4712

[21]. Iizumi T, Sakai T (2020) The global dataset of historical yields for major crops 1981–2016. Scientific Data 7:97. https://doi.org/10.1038/s41597-020-0433-7

[22]. Iizumi T, Yokozawa M, Sakurai G et al. (2014) Historical changes in global yields. Global

Ecology and Biogeography 23:346–357. https://doi.org/10.1111/geb.12120
[23]. Intergovernmental Panel on Climate Change (IPCC) (2021) Climate change 2021: the physical science basis. Contribution of Working Group I to the Sixth Assessment Report of the Intergovernmental Panel on Climate Change. In: Masson-Delmotte V, Zhai P, Pirani A et al. (eds) Cambridge University Press, Cambridge. https://www.ipcc.ch/assessment-report/ar6/ (accessed 18 February 2025)
[24]. Jägermeyr J, Müller C, Minoli S, Ray D, Siebert S (2021) GGCMI Phase 3 crop calendar [data set]. Zenodo. https://doi.org/10.5281/zenodo.5062513
[25]. Jägermeyr J, Müller C, Ruane AC et al. (2021) Climate impacts on global agriculture emerge earlier in new generation of climate and crop models. Nature Food 2:873–885. https://doi.org/10.1038/s43016-021-00400-y
[26]. Jägermeyr J, Müller C, Villoria NB et al. (2024) AgMIP Data Aggregator Tool. myGeoHub. https://doi.org/10.21981/1XJY-C362
[27]. Koo J, Anderson W (2023) What do we know about the impacts of the next El Niño on agrifood systems? CGIAR. https://www.cgiar.org/news-events/news/what-do-we-know-about-the-impacts-of-the-next-el-nino-on-agrifood-systems/ (accessed 18 February 2025)
[28]. Lange S (2021) ISIMIP3b bias adjustment fact sheet. https://www.isimip.org/documents/413/ISIMIP3b_bias_adjustment_fact_sheet_Gnsz7CO.pdf (accessed 18 February 2025)
[29]. Liaw A, Wiener M (2002) Classification and regression by randomForest. R News 2:18–22. https://journal.r-project.org/articles/RN-2002-022/ (accessed 18 February 2025)
[30]. Lin TS, Song Y, Lawrence P et al. (2021) Worldwide maize and soybean yield response to environmental and management factors over the 20th and 21st centuries. Journal of Geophysical Research Biogeosciences 126:e2021JG006304. https://doi.org/10.1029/2021jg006304
[31]. Liu W, Yang H, Folberth C et al. (2016) Global investigation of impacts of PET methods on simulating crop–water relations for maize. Agricultural and Forest Meteorology 221:164–175. https://doi.org/10.1016/j.agrformet.2016.02.017
[32]. Mauser W, Klepper G, Zabel F et al. (2015) Global biomass production potentials exceed expected future demand without the need for cropland expansion. Nature Communications 6:8946. https://doi.org/10.1038/ncomms9946
[33]. Mialyk O, Schyns JF, Booij MJ, Hogeboom RJ (2022) Historical simulation of maize water footprints with a new global gridded crop model ACEA. Hydrology and Earth System Sciences 26:923–940. https://doi.org/10.5194/hess-26-923-2022
[34]. Okada M, Iizumi T, Sakamoto T et al. (2018) Varying benefits of irrigation expansion for crop production under a changing climate and competitive water use among crops. Earth's Future 6:1207–1220. https://doi.org/10.1029/2017EF000763
[35]. R Core Team (2024) R: a language and environment for statistical computing. R Foundation for Statistical Computing, Vienna, Austria
[36]. Sacks WJ, Deryng D, Foley JA, Ramankutty N (2010) Crop planting dates: an analysis of global patterns. Global Ecology and Biogeography 19:607–620. https://doi.org/10.1111/j.1466-8238.2010.00551.x
[37]. Scafetta N (2022) Advanced testing of low, medium, and high ECS CMIP6 GCM simulations versus ERA5-T2m. Geophysical Research Letters 49:e2022GL097716. https://doi.org/10.1029/2022GL097716
[38]. Schewe, J., Gosling, S. N. & Reyer, C. et al. (2019) State-of-the-art global models underestimate impacts from climate extremes. Nature Communications, 10:1005.

https://doi.org/10.1038/s41467-019-08745-6
[39]. Singh J, Ashfaq M, Skinner CB et al. (2022) Enhanced risk of concurrent regional droughts with increased ENSO variability and warming. Nature Climate Chang 12:163–170. https://doi.org/10.1038/s41558-021-01276-3
[40]. Tilman D, Balzer C, Hill J, Befort BL (2011) Global food demand and the sustainable intensification of agriculture. Proc Natl Acad Sci USA 108:20260–20264. https://doi.org/10.1073/pnas.1116437108
[41]. Ubilava D (2017) The ENSO effect and asymmetries in wheat price dynamics. World Development 96:490–502. https://doi.org/10.1016/j.worlddev.2017.03.031
[42]. Vaittinada Ayar P, Battisti DS, Li C, King M, Vrac M, Tjiputra J (2023) A regime view of ENSO flavors through clustering in CMIP6 models. Earth's Future 11:e2022EF003460. https://doi.org/10.1029/2022EF003460
[43]. Webber H, Ewert F, Olesen JE et al. (2018) Diverging importance of drought stress for maize and winter wheat in Europe. Nature Communications 9:4249. https://doi.org/10.1038/s41467-018-06525-2
[44]. Welch BL (1947) The generalization of "Student's" problem when several different population variances are involved. Biometrika 34:28–35. https://doi.org/10.1093/biomet/34.1-2.28
[45]. You L, Wood S, Wood-Sichra U, Wu W (2014) Generating global crop distribution maps: from census to grid. Agricultural Systems 127:53–60. https://doi.org/10.1016/j.agsy.2014.01.002
[46]. Yu Q, You L, Wood-Sichra U et al. (2020) A cultivated planet in 2010 – Part 2: the global gridded agricultural-production maps. Earth System Science Data 12:3545–3572. https://doi.org/10.5194/essd-12-3545-2020
[47]. von Bloh W, Schaphoff S, Müller C et al. (2018) Implementing the nitrogen cycle into the dynamic global vegetation, hydrology, and crop growth model LPJmL (version 5.0). Geoscientific Model Development 11:2789–2812. https://doi.org/10.5194/gmd-11-2789-2018

ELECTRONIC SUPPLEMENTS

LIST OF FIGURES AND TABLES IN THIS FILE

Table S1. List of the GCMs, modeling groups and equilibrium climate sensitivity (ECS) obtained from the CMIP6 multi model ensemble dataset (Eyring et al. 2016) for this study. The ECS values are taken from Scafetta (2022).

Model name	Modeling group	ECS (°C)
GFDL-ESM4	National Oceanic and Atmospheric Administration, Geophysical Fluid Dynamics Laboratory, USA	3.90
IPSL-CM6A-LR	Institut Pierre Simon Laplace, France	4.56
MPI-ESM1-2-HR	Max Planck Institute for Meteorology, Germany	2.98
MRI-ESM2-0	Meteorological Research Institute, Japan	3.15
UKESM1-0-LL	Met Office Hadley Centre, UK	5.34

Table S2. A summary of the performance statistics calculated between the climate-crop model ensemble and actual data in the historical period (1983–2020). The statistics include the total number of grid cells where both simulated and observed data are available for comparison (Ngrids), the Pearson correlation coefficient calculated between the simulated and actual data across all grid cells regardless of the significance of yield impact (Corr), the Cohen's Kappa coefficient, which measures the agreement between simulated and actual data categorized as either positive or negative yield impact regardless of the significance of yield impact (Kappa). The number of grid cells, correlation coefficient, and Kappa coefficient are also calculated using the grid cells with significant yield impact at the significance level of 10% (i.e., the p-value <= 0.1) are also shown (Corr_lowP, Kappa_lowP, and N_grids_lowP).

Crop	**Phase**	**Corr**	**Pvalue**	**Kappa**	**Ngrids**	**Corr_lowP**	**Pvalue_lowP**	**Kappa_lowP**	**Ngrids_lowP**
wheat	El Niño	0.061	0.0	0.023	6538	-0.033	0.716	0.172	122
wheat	La Niña	0.143	0.0	0.036	4753	0.714	0.0	0.591	110
rice	El Niño	0.054	0.0	0.045	5796	-0.001	0.992	0.009	181
rice	La Niña	0.073	0.0	-0.013	3207	0.279	0.0	0.251	160
maize	El Niño	0.199	0.0	-0.029	6544	0.625	0.0	0.502	205
maize	La Niña	0.126	0.0	0.102	4182	0.287	0.026	0.457	60
soybean	El Niño	-0.353	0.0	-0.191	2905	-0.78	0.0	-0.413	22
soybean	La Niña	-0.218	0.0	-0.233	2078	-0.39	0.001	-0.126	67

Table S3. The number of grid cells where the different sources of yield impact estimates are available in the historical period (1983–2020). The category "Both" indicates both the actual and climate-crop model ensemble data are available, while "Only" indicates that either the actual or the model ensemble data is available. The values in the parenthesis indicate the percentages relative to the total number of grid cells with the model ensemble data.

Crop	Phase	ssp126	Actual	Both	ssp126_Only	Actual_Only
wheat	El Niño	20901	11552 (55%)	11303 (54%)	9598 (46%)	249
wheat	La Niña	20901	7798 (37%)	7590 (36%)	13311 (64%)	208
rice	El Niño	10862	8491 (78%)	7133 (66%)	3729 (34%)	1358
rice	La Niña	10862	8480 (78%)	7103 (65%)	3759 (35%)	1377
maize	El Niño	15318	10281 (67%)	7483 (49%)	7835 (51%)	2798
maize	La Niña	15318	9623 (63%)	6932 (45%)	8386 (55%)	2691
soybean	El Niño	10193	4472 (44%)	4036 (40%)	6157 (60%)	436
soybean	La Niña	10193	3499 (34%)	3137 (31%)	7056 (69%)	362

Table S4. Global area-weighted average yield anomalies. In this table, “Avg_AreaYield_E,” “Avg_AreaYield_N,” and “Avg_AreaYield_L” represent the average percentage yield anomalies for El Niño, Neutral, and La Niña conditions, respectively. These averages are derived by weighting grid-level yield anomalies by the harvested area.

Crop	**Period**	**Scenario**	**Avg_AreaYield_E (%)**	**Avg_AreaYield_N (%)**	**Avg_AreaYield_L (%)**
wheat	1983_2020	actual	-2.49	-0.11	-4.26
wheat	1983_2020	ssp126	0.96	-0.09	-2.00
wheat	2035_2064	ssp126	-0.34	-0.09	-0.34
wheat	2035_2064	ssp585	-0.82	0.23	-0.15
wheat	2065_2094	ssp126	0.39	0.00	0.92
wheat	2065_2094	ssp585	-0.73	0.12	0.95
soybean	1983_2020	Actual	1.11	-0.72	-0.11
soybean	1983_2020	ssp126	1.50	0.05	-1.15
soybean	2035_2064	ssp126	0.20	-0.13	-0.22
soybean	2035_2064	ssp585	1.12	0.13	0.53
soybean	2065_2094	ssp126	1.05	-0.01	1.33
soybean	2065_2094	ssp585	1.46	-0.62	0.96
rice	1983_2020	Actual	-1.61	0.24	-1.19
rice	1983_2020	ssp126	-1.61	0.09	1.62
rice	2035_2064	ssp126	-1.39	0.09	2.09
rice	2035_2064	ssp585	-1.99	0.14	0.55
rice	2065_2094	ssp126	-1.85	-0.05	1.22
rice	2065_2094	ssp585	-1.24	-0.02	1.52
maize	1983_2020	Actual	-3.06	0.09	-0.09
maize	1983_2020	ssp126	-1.04	0.19	0.75
maize	2035_2064	ssp126	-1.34	0.16	0.71
maize	2035_2064	ssp585	-1.59	0.13	0.48
maize	2065_2094	ssp126	-1.77	-0.06	0.95
maize	2065_2094	ssp585	-0.60	-0.13	0.93

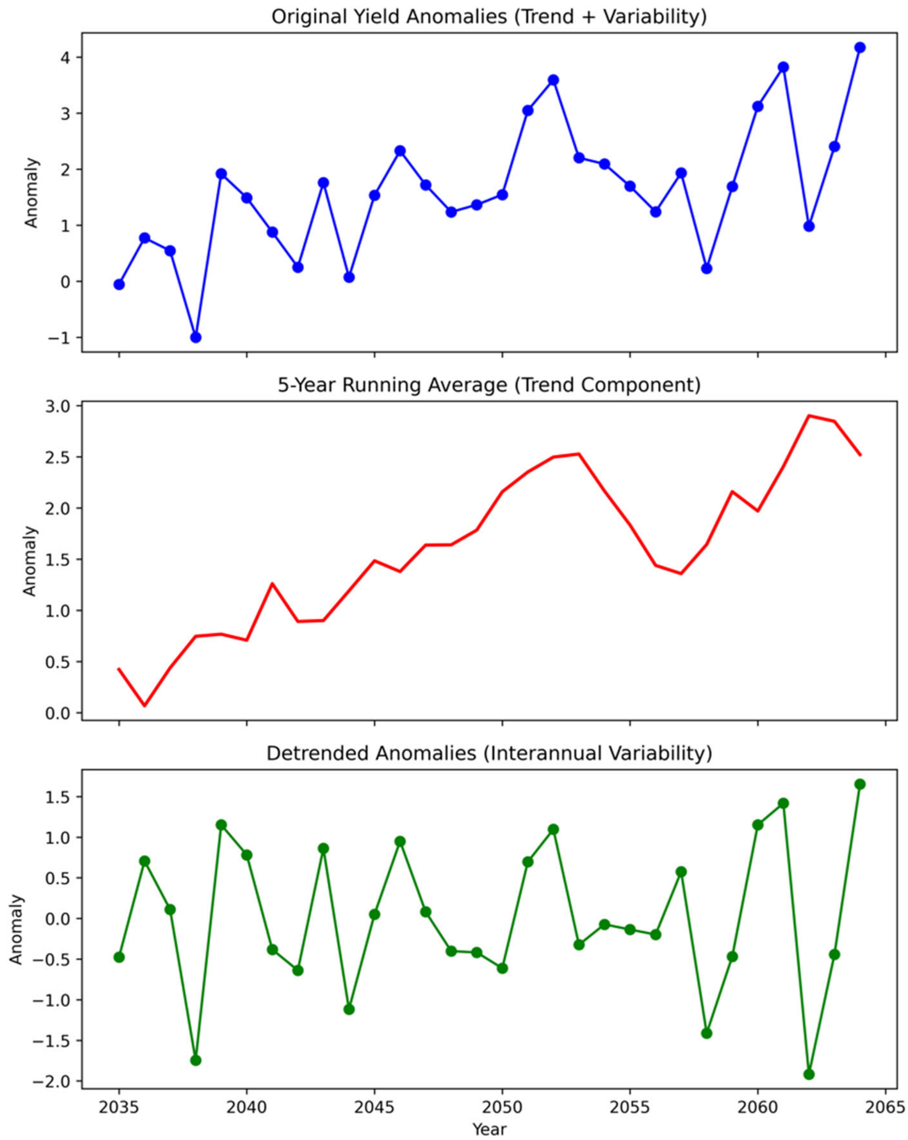

Fig. S1. Detrending of annual yield time series. The original yield time series (top), trend component represented by 5-year running average (middle) and interannual variability component or yield anomalies (bottom). The data shown here is artificially generated for explanation purposes.

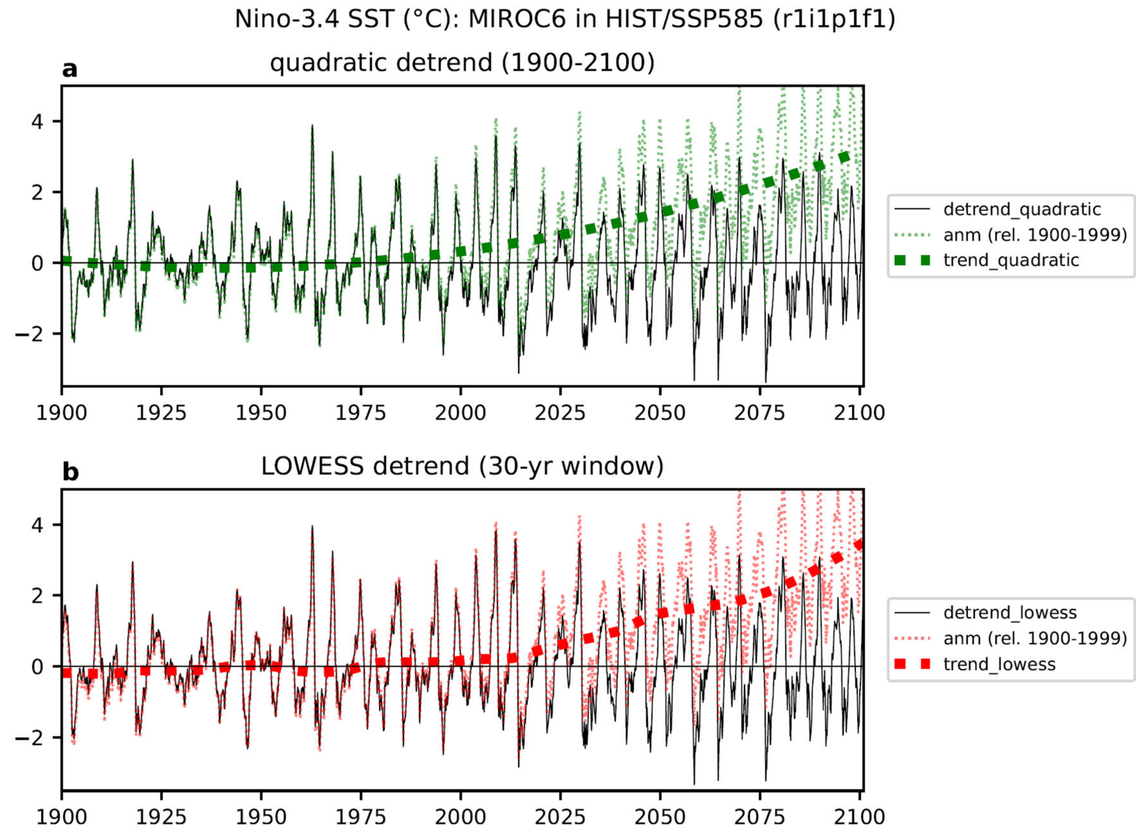

Fig. S2. An example of Nino3.4 monthly SST anomaly series derived from a GCM.

595
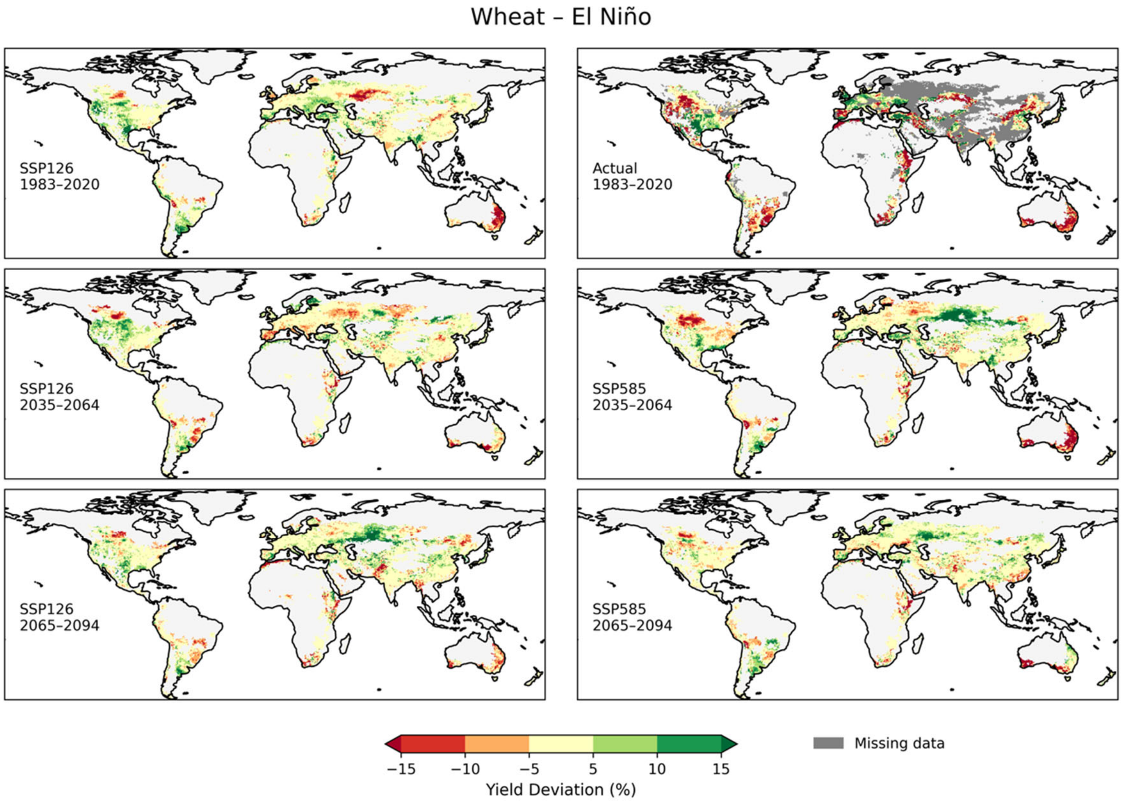

596 Fig. S3. Same as Fig. 2 but for wheat in the El Niño years.
597

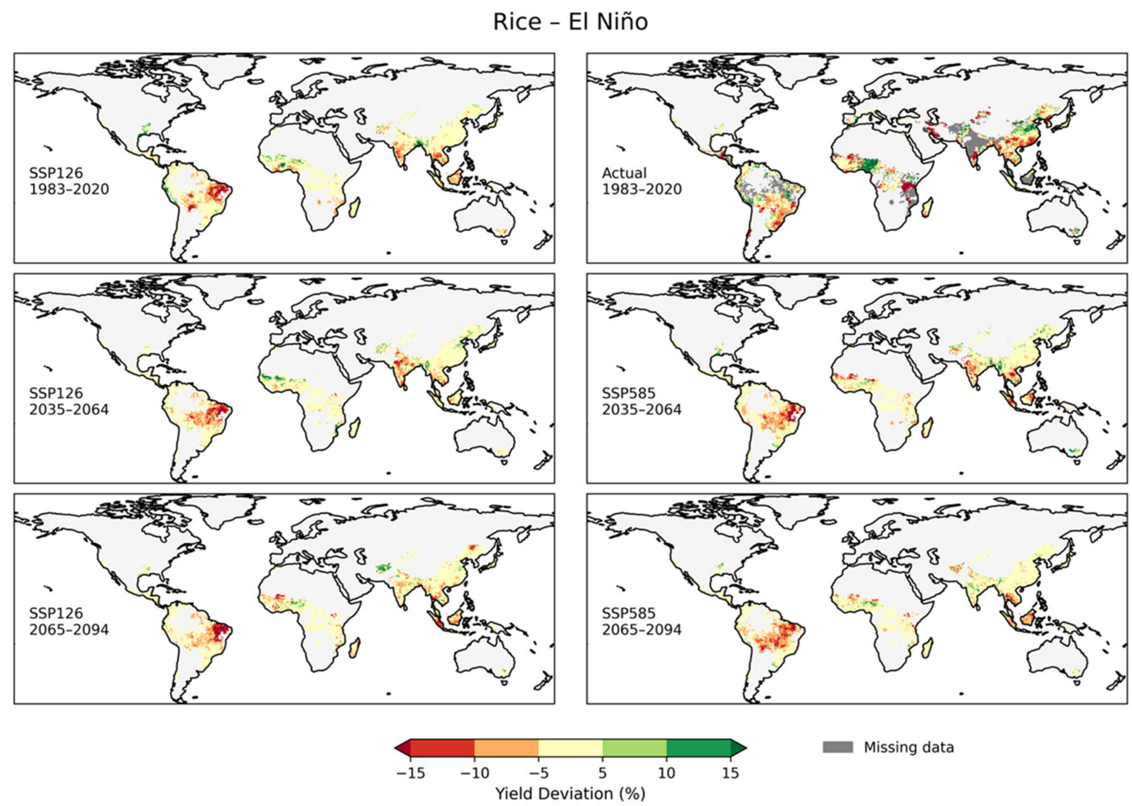

Fig. S4. Same as Fig. 2 but for rice in the El Niño years.

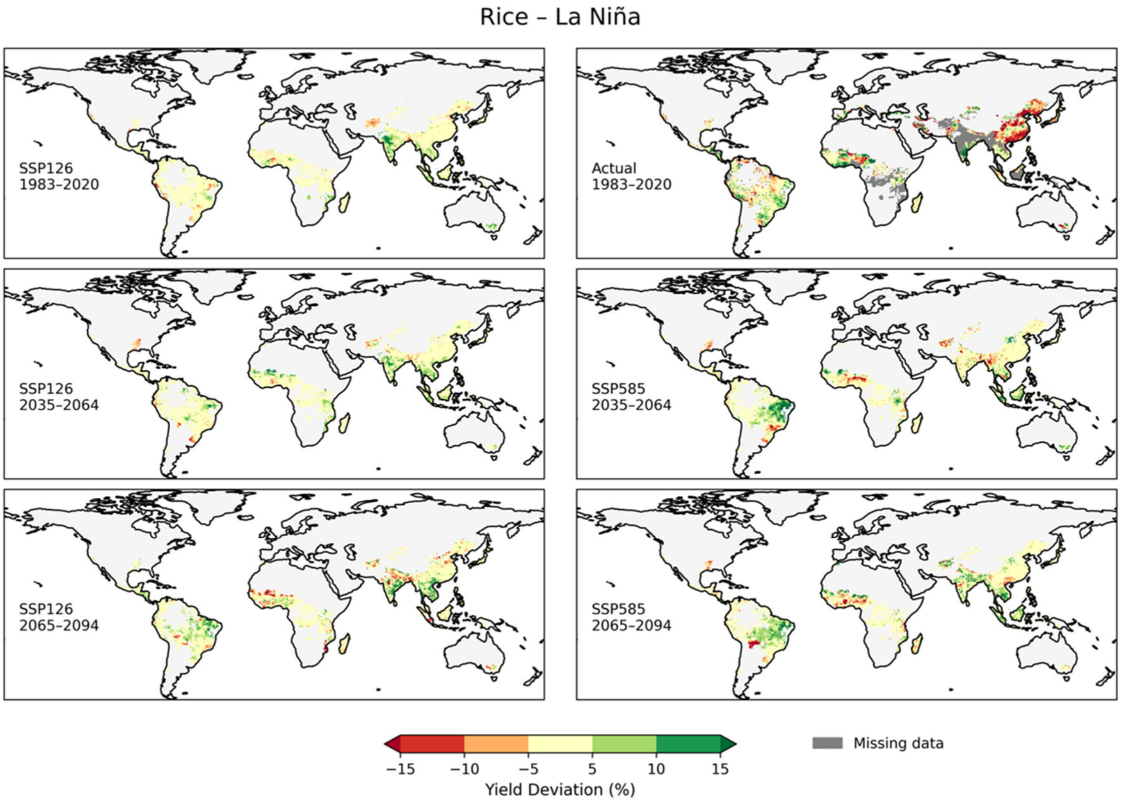

601
602 Fig. S5. Same as Fig. 2 but for rice in the La Niña years.

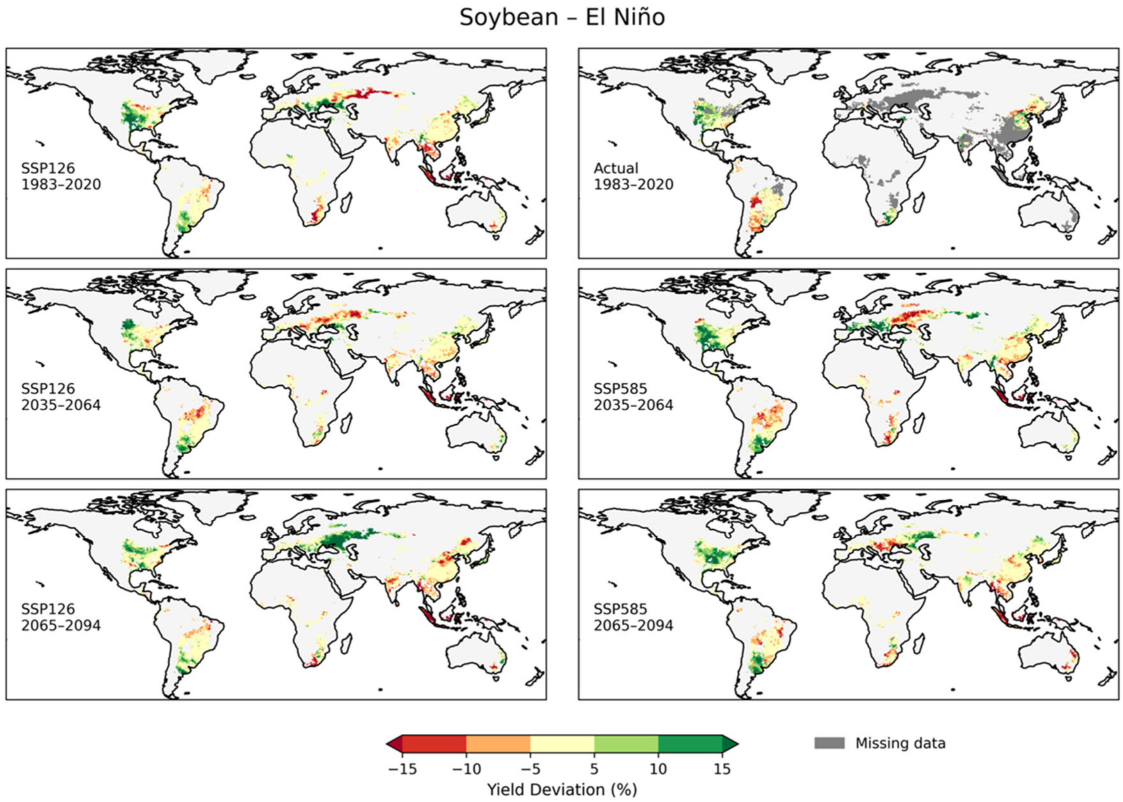

Fig. S6. Same as Fig. 2 but for soybean in the El Niño years.

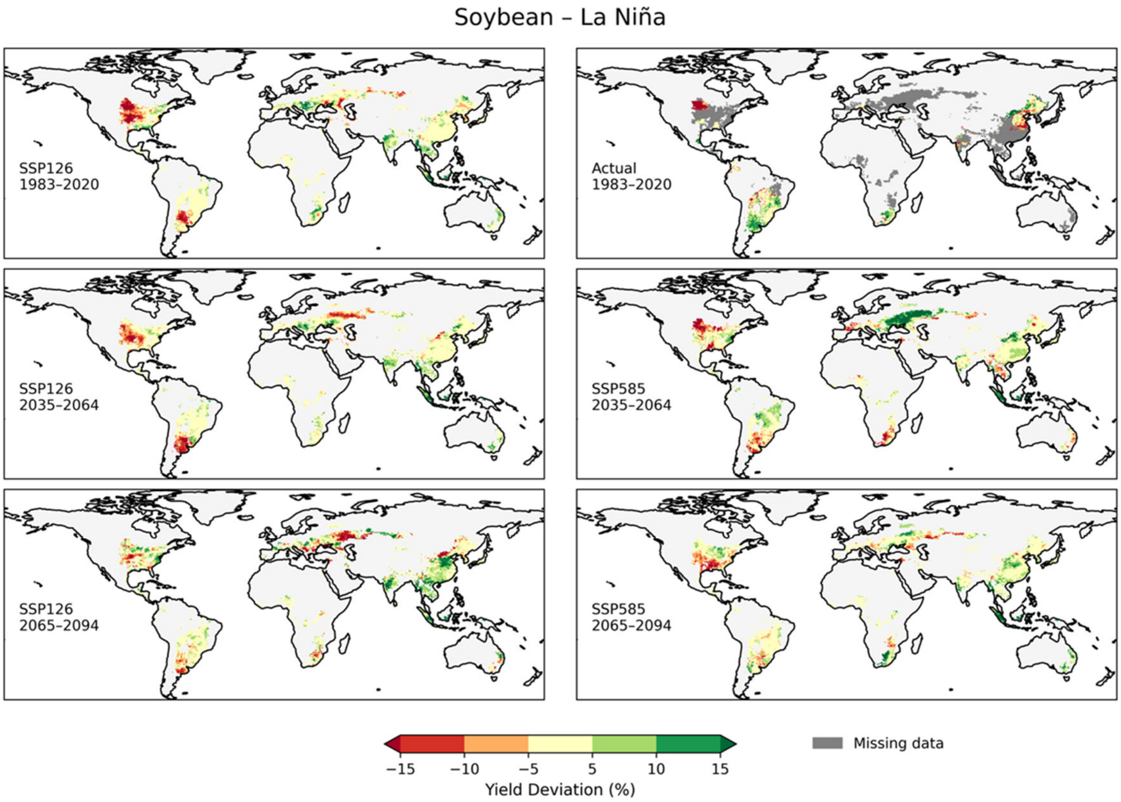

606
607 Fig. S7. Same as Fig. 2 but for soybean in the La Niña year.